A Hybrid Controller Assisted Voltage Regulation and Power Splitting Strategy for Battery/Supercapacitor System in Isolated DC Microgrid

Arunkumar C R, *Graduate Student Member, IEEE*, and Udaya Bhasker Manthati, *Member, IEEE*

***Abstract*—The hybrid energy storage system (HESS) on a direct current (DC) microgrid aims to ensure rapid and accurate dc bus voltage control. However, the conventional control approaches are challenging to implement with minimal setting time and overshoot, which can cause significant variations in dc bus voltage. The PI controllers used in traditional techniques add an extra lag to the control loop and increase the difficulty of parameter tuning. Additionally, using a power splitting scheme based on a traditional first-order low-pass filter (LPF) delays the control loop and slows down system dynamics. To address this issue, a hybrid control strategy that employs a proportional-integral controller for dc bus voltage control and a simple prediction control for duty calculation is proposed in this work. An improved power splitting scheme is incorporated for HESS, which reduces the effect of LPF on the battery current reference calculation and enhances the dynamics of the dc microgrid. Furthermore, a voltage regulation loop is added to guarantee the charging of the SC without affecting the dc microgrid operation. The proposed method is validated through detailed simulation and experimental studies that show improved dc bus voltage control and HESS power-sharing.**

***Index Terms*—Energy storage system, power sharing, dc microgrid, battery, hybrid controller, energy management.**

I. Introduction

RENEWABLE energy sources (RES) for power generation have become more popular due to environmental concerns such as global warming, rising fuel prices in recent years, and the imminent depletion of fossil fuels [1]. Nevertheless, one of the most crucial challenges in implementing RES is the intermittent and non-dispatchable characteristics causing power quality concerns in the clean power generated [2], [3]. Energy storage devices address this issue by supplying/absorbing load demand when load power is scarce or surplus. To store energy, various kinds of energy storage systems (ESS) are used, including battery energy storage systems (BESS) [4], [5], pumped hydro electric storage systems [6], and fuel cell systems [7]. Compared to other energy storage systems, BESS is one of the most appealing storage solutions in the power sector due to its low cost and reasonable size.

The BESSs have a crucial feature: high energy density, making them an effective device for controlling energy vacillations. Nevertheless, the BESSs have low power densities, resulting in ineffective storage when power variations are significant and rapid [8]. Such high power fluctuations can cause severe damage to the battery banks and shorten the battery life cycle in the long run. Furthermore, if large power fluctuations are not adequately supplied, they can harm power quality, leading to the failure of electrical loads [9], [10]. SC, on the other hand, is being actively researched and widely perceived as a fast, responsive energy storage technology due to its desirable features such as high power density and long life span [11]. Although the energy density is very low, they offer other advantages such as a wide operating temperature band, low internal resistance, and high efficiency [12]. As a result, the battery banks combine with an SC, allowing instantaneous current to be redirected from the battery. The combined HESS possesses both high energy density and high power density.

The HESS connects to dc microgrid through three main configurations. The basic HESS structure is a passive configuration with a direct connected SC and battery to the dc bus [13]. The semi-active configuration includes actively and passively connected storage devices [14], [15]. The active energy storage is connected to the dc microgrid through a power electronic converter. The loss in passive/ semi-active configuration is less due to the reduced number of power converters. Regardless, the absence of control over passive energy storage limits the effective use and power-sharing of HESS. The HESS is integrated with the dc microgrid using fully active topologies, enabling control over the power flow in the HESS [16].

Significant research has been conducted and published in the literature in the field of developing control mechanisms for a HESS based dc microgrid [17], [18], [19], [20], [21], [22], [23], [24], [25], [26], [27], [28], [29], [30]. The traditional control of fully active HESS follows a two-loop structure [17]. The inner loop controls the HESS current, regulating the dc bus voltage. A low order filter divides the total HESS reference current by the average battery reference current and the transient SC reference current [18], [19]. A grid integrated PV-dc microgrid

Manuscript received 16 April 2022; revised 3 November 2022 and 12 February 2023; accepted 15 April 2023. Date of publication 25 April 2023; date of current version 22 August 2023. Paper no. TEC-00384-2022. *(Corresponding author: Arunkumar C R.)*

Arunkumar C R is with the Research Scholar, Electrical Engineering Department, National Institute of Technology, Warangal 506004, India (e-mail: acr_research@student.nitw.ac.in).

Udaya Bhasker Manthati is with the Electrical Engineering Department, National Institute of Technology, Warangal 506004, India (e-mail: ub@nitw.ac.in).

Color versions of one or more figures in this article are available at https://doi.org/10.1109/TEC.2023.3270292.

Digital Object Identifier 10.1109/TEC.2023.3270292

system is proposed with a unified controller for the bidirectional power flow in HESS [20]. This article selects operating modes based on the power difference between PV output and load demand. However, a fixed power-sharing coefficient was used. A faster joint control strategy-based dc microgrid for faster dc-link voltage regulation has been proposed in [21]. This article diverts the uncompensated battery currents to the supercapacitor for enhanced dynamic performance. The battery current based reference generation for HESS is proposed for an autonomous dc microgrid in [22]. Though these methods improve the overall dynamics in the system, the direct connected low pass filter in the battery control loop adds delay to system dynamics.

Nevertheless, dual-loop control methods based on PI cannot produce an optimal transient response; Instead, they result in a shorter settling time and a higher overshoot or vice versa. Furthermore, a shorter settling time in the PI controller generates a more significant overshoot due to parameter adjustment issues, and designing a three-loop PI controller with six parameters increases the complexity of controller design [23], [24]. The above schemes use conventional LPF for power distribution, increasing the control system's delay and battery reference current tracking.

Advanced and sophisticated control strategies introduce to control the HESS in dc microgrid. The sliding mode control (SMC) is used to obtain fast dynamic performance and combined with other controllers to improve the system performance. However, conventional SMC methods are affected by chattering [25], [26] and modified SMC techniques requires complex modelling [27]. Fuzzy logic controllers (FLC) have incorporated power management strategies in HESS for better power allocation and dc bus regulation. However, FLC system performance relies on human knowledge, and it requires regular updating of data [28]. The model predictive control shows promising performance for HESS-assisted dc microgrid [29], [30]. In [29], a multi-input converter assisted HESS in implementing isolated dc microgrid applications. The MPC-based topology improves the system dynamics and power-sharing in HESS. Though, they require faster processors and optimization techniques to implement.

This article proposes a two-level hybrid control strategy and power-sharing scheme for HESS in an isolated dc microgrid. In a conventional power-sharing scheme, a first-order low pass filter is directly connected to the battery controller, increases the delay in the control loop, and causes slow system dynamics. Further, the lag nature of the PI controller adds delay to the control system. Hence, a two-level hybrid controller is proposed, featuring fast predictive control for current regulation and a slow PI controller for voltage regulation. The simple duty calculation control reduces the tuning burden and provides faster dynamics for HESS current regulation. The current predictive control calculates the duty signal in one sampling period, reducing the computational burden. The proposed power splitting scheme for battery and SC is introduced such that it generates battery reference current without the aid of LPF. It reduces the delay in battery reference current calculation and the over-discharge of the battery during the steady state. Further, the proposed method reduces the effort of parameter tuning, and a slow outer voltage controller ensures that the dc bus voltage is unaffected by sudden disturbances and noises. A second controller is incorporated as a long-term solution to charge the SC in both steady-state and transient conditions. The suggested SC charging approach have less impact on the charge/discharge rate of battery current and dc bus voltage regulation. The following list summarises the main ideas and steps involved in this work:

1) This article proposes a hybrid controller with a new power-splitting scheme for HESS in a PV-fed dc microgrid. While the slow dynamics of the PI controller regulate the dc bus voltage, the discrete nature of duty calculation enables fast dynamics and accurate tracking of HESS reference currents. Furthermore, the hybrid controller calculates the required duty in one sample time and reduces the computational burden in the system.
2) The proposed HESS hybrid control follows a simple three-loop structure with external voltage control to regulate dc bus voltage and two predictive control loops for tracking the reference currents. It requires only two parameters to be adjusted for dc bus voltage regulation, reduces the complexity of tuning and settles the dc microgrid faster.
3) In the battery control loop, the proposed power-sharing method eliminates the use of LPF directly. As a result, it ensures accurate battery current tracking and reduces control loop delay.
4) A controlled charging scheme for SC is incorporated to charge SC from the dc bus during regular operation. The Controlled scheme enables charging of SC at regular operation and supplies transient power at the time of disturbances.
5) A detailed controller modelling and analysis are presented to validate the hybrid controller. Further, the controller is tested with simulation ad experimentally for various conditions.

Paper presented in the following order: Section II discusses dc microgrid configuration and conventional controller. Section III explains the proposed control strategy. Simulation study is presented in Section IV and hardware results are discussed in Section V. Section VI concludes the work.

II. DC Microgrid Configuration and HESS Control Strategy

The proposed autonomous dc microgrid configuration is depicted in Fig. 1. One unidirectional boost converter and two bidirectional boost converters are utilized to incorporate the photovoltaic (PV) panel, battery and supercapacitor into the dc bus. The HESS converters have a bidirectional property to enable power flow in both directions. The bttery, SC and PV converter filter inuctance are represented by L_b, L_{sc}, L_{pv} respectively, and output filter capacitance is denoted by C_0. The V_{pv}, V_{sc}, V_b, and V_0 are the PV, battery, supercapacitor and load bus voltage respectively. The power converter switches are represented by S_{pv}, S_{b1}, S_{b2}, S_{sc1}, and S_{sc2} and D represents the PV converter diode. The PV panel is controlled to extract maximum power using Perturb and Observe (P&O) based power point tracking (MPPT) control. dc microgrid operation can be classified into deficit power mode (DPM) and excess power mode (EPM).

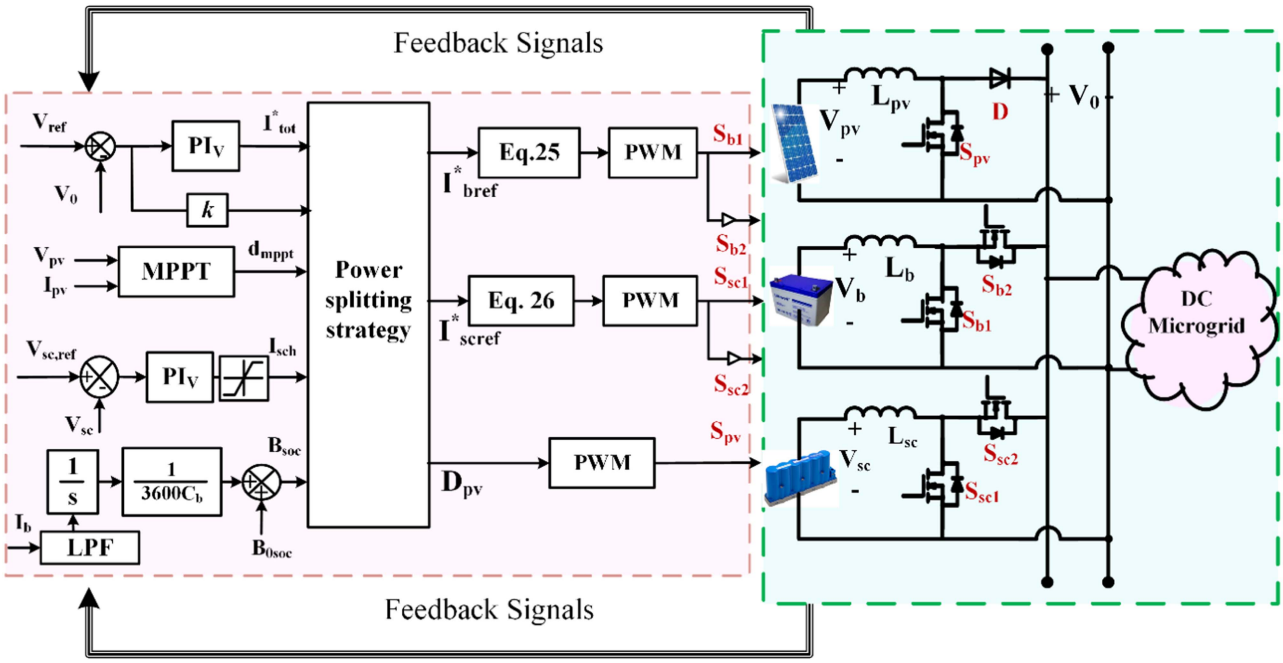

Fig. 1. Architecture of isolated DC microgrid and control.

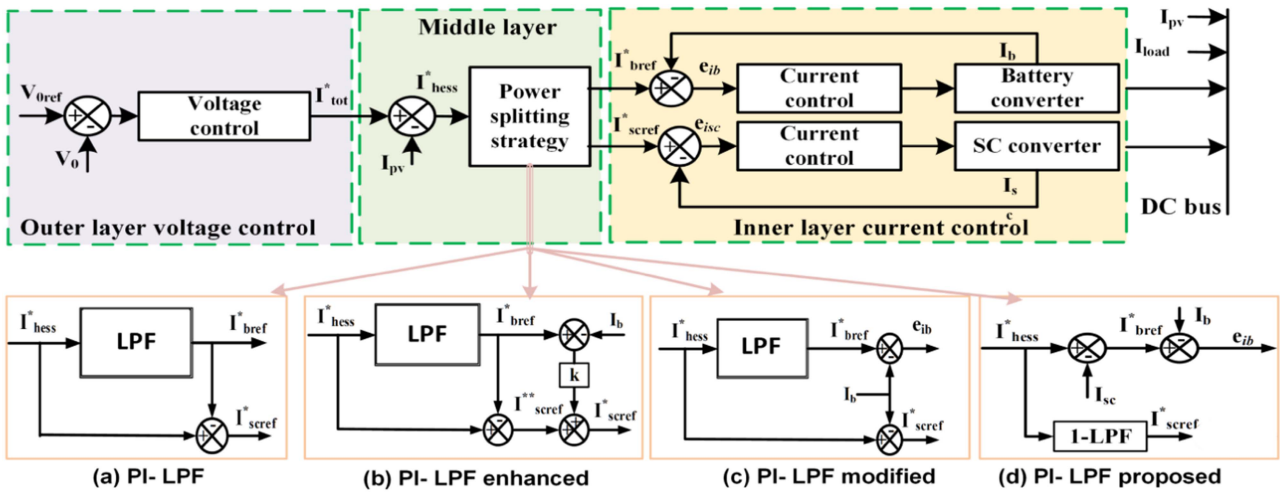

Fig. 2. Three layer HESS control structure and different power splitting schemes; different power splitting strategies: (a) conventional LPF (b) enhanced LPF by adding battery error current (c) modified LPF based on battery current (d) proposed LPF based on SC current.

When PV generation exceeds load requirements, the HESS absorbs the excess power from the dc load bus, referred to as EPM. During PV generation is less than the load demand, the dc microgrid operates in DPM, and the additional power flows from HESS to the dc bus.

The HESS control for the dc microgrid follows a three-layer structure as shown in Fig. 2. The outer layer of the three-layer structure generate the reference current to regulate dc microgrid voltage. Based on errors in battery and SC currents, the inner layer calculates the control signal/duty signal. The middle layer of the HESS control scheme derives the battery and SC reference currents from the total HESS reference current generated by the outer layer.

The performance of HESS depends on the power-sharing strategy used in the middle layer. The lower order LPF based power splitting scheme is most used in literature to reduce the complexity of the middle layer, and the cut-off frequency selected for LPF is 5 Hz. The basic LPF power spitting strategy follows battery current reference generation by bypassing the total HESS current through LPF. The difference between the LPF output signal and input signal gives the SC reference current as shown in Fig. 2(a). The basic LPF power-sharing scheme is enhanced by adding uncompensated battery current to the SC as given in Fig. 2(b). It reduces the ripple in battery current and dc bus voltage. Another method used for generating the reference current for battery and SC utilizes actual battery current as shown

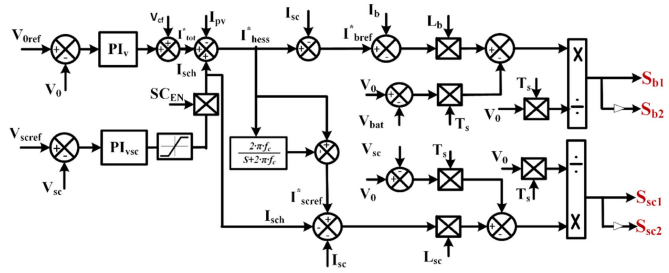

Fig. 3. Block diagram of proposed hybrid controller with SC charging scheme.

in Fig. 2(c). In this method, the battery current reference is the output of LPF and SC current reference is the difference between the HESS current reference and the actual battery current. In all the above methods, the LPF is directly connected to the battery control loop, which leads to over-discharge of the battery and slow dynamics in the load voltage. Hence in this work, we propose a simple power-sharing strategy to minimize the direct use of LPF in the HESS control loop, as shown in Fig. 2(d). In the proposed method, the battery reference current is generated from SC current without the aid of LPF. Following describes the detailed analysis of proposed control and power splitting scheme.

III. Proposed Control Strategy

The dc microgrid control has two parts via PV module control and HESS control. The PV module uses perturb and observe (P&O) MPPT technique to extract the maximum power from solar panels. The HESS requires separate controllers to regulate dc bus voltage and power balancing. The traditional HESS control strategy follows a dual loop structure with PI controllers. However, it demands to tune three PI controllers with six parameters to obtain optimum performance. On the other hand, the proposed hybrid controller requires tuning of only two parameters and uses the speed of prediction control, as shown in Fig. 3. The PI controller is designed to regulate the dc bus voltage, and the predictive control is used to control the HESS currents. The battery and SC current reference are generated using an LPF decoupling strategy. The main functions of the HESS control scheme are i) generation of total current reference for dc buss regulation, ii) battery and SC power sharing during transient and steady state period iii) generation of modulating signals for power converter based on prediction and iv) control of SC voltage and battery state of charge regulation.

A. Control of PV Module

This work uses the basic P&O MPPT technique to control PV panels. In the P & O algorithm, the duty signal is controlled in steps to reach the maximum power point. First, the PV power (δP_{PV}) and PV voltage (δV_{PV}) variations with previous samples are recorded and then compared to produce the duty pulse for the next instant [8].

B. Power Balance and Reference Generation

The total dc microgrid current reference is generated by outer voltage controller (PI_v) based on error in dc bus voltage. Battery and SC reference current are decided by proposed power sharing strategy. The total power balance in the system can be written as:

$$P_L(t) = P_{PV}(t) + P_{bat}(t) + P_{sc}(t) = P_{avg}(t) + P_{tr}(t) \quad (1)$$

Where $P_{PV}(t), P_{bat}(t), P_{sc}(t), P_L(t)$ are the power supplied by PV, power supplied/absorbed by battery and SC and power absorbed by load. The average and transient power demand is represented by $P_{avg}(t)$ and $P_{tr}(t)$. The charging of supercapcitor is controlled by SC_{EN}. Under SC charging, SC_{EN} made unity. $P_{sc,ch}(t)$ is the charging power of SC.

$$P_{PV}(t) + P_{bat}(t) = P_L(t) + P_{sch}(t) \quad (2)$$

$$P_{sch}(t) = -P_{sc} \quad (3)$$

The $P_{sch}(t)$ is positive during charging and negative during discharging. The total HESS current reference including SC charging current can be given as:

$$i^*_{hess} = i^*_{bref} + i^*_{sc} = i^*_{tot} - i_{pv} + V_{cf} + i_{sch} \cdot SC_{EN} \quad (4)$$

Where, V_{cf} is the voltage compensation factor used to improve the dynamic performance of microgrid. It can be represented in discrete form as

$$V_{cf}(k) = G * dv + V_{cf}(k-1) \quad (5)$$

Where $dv = V_{0ref} - V_0$ and G is the voltage compensation gain. G is selected in such a way that $G = 0$ for $dv > 1$ and a small positive number less than 1 for $dv < 1$. The feedback of the previous state allows reducing the Bus voltage error. The total HESS reference current is split into the battery and SC reference current using the power splitting strategy.

$$i^*_{hess} = i^*_{bref} + i^*_{scref} \quad (6)$$

Where,the total current reference is i^*_{tot}, SC current reference is i^*_{scref}, battery current reference is i^*_{bref} and total HESS current reference is i^*_{hess}. The average battery current component of HESS current by considering charging is calculated by:

$$i^*_{bref} = i^*_{hess} - i_{scref} \quad (7)$$

$$i^*_{scref} = i^*_{hess}(1 - LPF) \quad (8)$$

The LPF with cutoff frequency f_c is given by:

$$LPF = \frac{2 \cdot \pi \cdot f_c}{s + 2 \cdot \pi \cdot f_c} \quad (9)$$

The main aim of LPF in the proposed method is to generate supercapacitor reference current. A high value of f_c leads to poor operation of supercapacitor unit. Also, a low value of f_c leads to sluggish response in the control system. Hence based on literature and simulation, the f_c is selected as 5 Hz [21].

C. HESS Converter Duty Signal Generation

The duty calculation is a simple method to get the required duty to regulate the dc microgrid. To regulate the HESS currents, the inductor equations are used to calculate the duty. The battery and SC inductor current average equations can be given as:

$$\frac{(di_b(t))L_b}{dt} = V_{bat}(t) - (1 - d_b(t)V_0(t)) \tag{10}$$

$$\frac{(di_{sc}(t))L_{sc}}{dt} = V_{sc}(t) - (1 - d_{sc}(t))\, V_0(t) \tag{11}$$

After expanding (10) and (11) using euler's difference law [29];

$$\frac{(i_b(k+1) - i_b(k))L_b}{T_s} = V_{bat}(k) - (1 - d_b(k))V_0(k) \tag{12}$$

$$\frac{(i_{sc}(k+1) - i_{sc}(k))L_{sc}}{T_s} = V_{sc}(k) - (1 - d_{sc}(k))V_0(k) \tag{13}$$

From the perspective of discrete control, (12) and (13) can be rearrange to obtain control signals d_{sc} and d_b. The battery $(i_b(k+1))$ and SC $(i_{sc}(k+1))$ reference currents can be rewritten as I^*_{bref} and I^*_{scref} [29]. The kth state represents the feedback signals from the dc micorgird.

$$d_b(k+1) = \frac{L_b(I^*_{bref} - I_b + T_s(V_0(k) - V_{bat}(k)))}{T_s V_0} \tag{14}$$

$$d_{sc}(k+1) = \frac{L_{sc}(I^*_{scref} - I_{sc}) + T_s(V_0(k) - V_{sc}(k))}{T_s V_0} \tag{15}$$

The duty pulses are generated by comparing calculated control signals d_b and d_{sc} with a sawtooth carrier wave. The period of the carrier signal is T_s. The duty calculation determines the required modulating signal in one cycle, which reduces the computational burden and improves the dynamics of the control system. The block diagram representation of overall hybrid control system is depicted in Fig. 3.

D. dc Bus Voltage Control

The voltage control loop calculates the required reference current based on the dc bus voltage error. The boost converter model has a right-hand plane zero (RHPZ) in the voltage control transfer function, leading to undesirable fluctuations in bus voltage [22]. Hence, special care must be taken while choosing the outer voltage control loop bandwidth for PI controller design. The single input, single output tool (SISO tool) in MATLAB [21] and the overall transfer function without the controller are used to tune the PI controller parameters. The phase margin of 60° and bandwidth of 700 rd/sec are selected to ensure stable voltage regulation [22]. $k_p = 0.25$ and $k_i = 160$ are the calculated values.

E. SC Voltage Regulation

An extra voltage controller is added to regulate the SC voltage. The charging is active only if $SC_{EN} = 1$.SC operating voltage can change from 100% to 0% depending on the power requirement during operation. However, the useful energy varies nonlinearly concerning the reduction in voltage. For example, 75% of useful energy is dissipated when SC voltage reduces to 50%. Thus the lower operating range of SC voltage is limited to 50%. Below 50%, the SC_{EN} enables to charge of the SC unit. The charging current required for SC (I_{sch}) is added to the i^*_{tot} so that the sudden change in system current is split between battery and SC as shown in Fig. 3. The charging current is decided by the SC voltage control PI and saturation limit. The PI values selected as K_{psc}= 0.2 and K_{isc}= 5. The new HESS reference current for HESS considering SC charging current is given by:

$$i^*_{hess} = I^*_{tot} - I_{pv} + I_{sch}SC_{EN} \tag{16}$$

The new SC reference current is given by:

$$i^*_{scref} = i^*_{tot} - i^*_{bat} - I_{sch}SC_{EN} \tag{17}$$

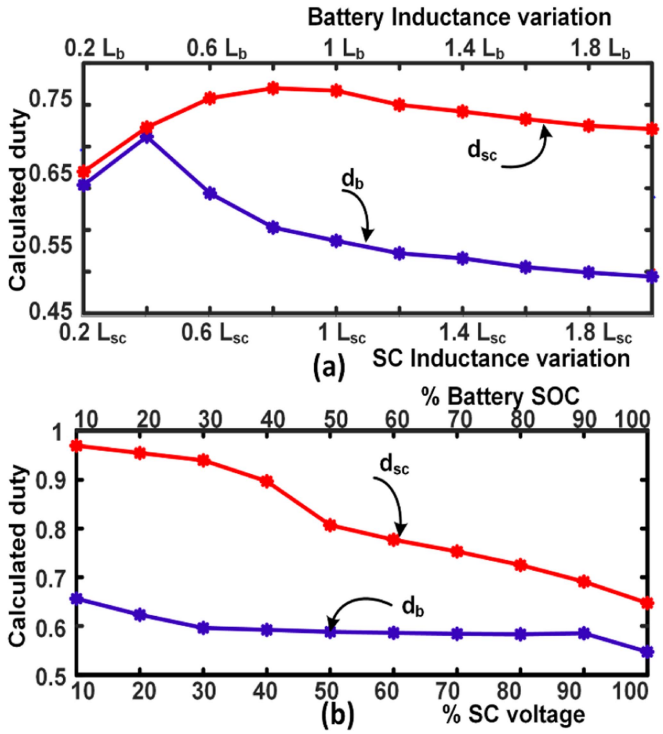

Fig. 4. Dependency of battery and SC on system parameter variation (a) converter inductance variation (b) battery SOC variation and SC voltage variation.

F. Analysis of Dependency on Parameter Variation

This section analyzes the effect of parameter variation on calculated duty. Fig. 4 shows the average value of calculated duty for battery and SC converter. From (14) and (15), the duty mainly depends on converter filter inductance, battery voltage, and SC voltage. The calculated duty is plotted against each parameter by considering other parameters are at 80%.

The battery voltage will be almost constant irrespective of the state of charge (SOC). Hence, the variation in calculated duty is limited to 0.55 to 0.65 as battery SOC varies. The variation in the calculated duty of the battery and SC converter concerning converter inductance is shown in Fig. 4(a). The plot shows that reducing inductance increases the duty to supply the required

TABLE I
SIMULATION PARAMETERS FOR DC MICROGRID SYSTEM

S.No	Parameter	Values
1	Battery unit	V_{bat}= 48 V, 21 Ah
2	Supercapacitor unit	V_{sc}= 48 V, C_{sc}=19.3F
3	PV panel	V_{pv}= 60 V, I_{pv}=14.7 A
4	DC-DC converters	L_{sc}=2.3 mH,L_b=2.3 mH, L_{pv}= 3.1 mH, C_{0dc}=430 μF
5	Rated output power, P_{out}	1 kW
6	Switching Frequency, f_{sw}	20 kHz
7	Load Voltage, V_0	96 V

current. Further, an increase in inductance than the designed value has less effect on duty. The calculated duty variation for battery SOC and SC voltage level is plotted in Fig. 4(b). The calculated SC duty varies between 0.6 to 0.96. The calculated SC converter duty increases above 0.8 as SC operating voltage falls below 50%. Because, at lower SC voltage, it requires high duty to regulate the load voltage. It is important to note that the duty increases to the upper peak as the SC voltage lowers. Sometimes this may lead to duty saturation in a practical scenario. Hence, fixing the lower limit of SC voltage during operation is essential. The charging of SC is added in this work to address this issue such that SC charging enables below 50% of SC voltage.

IV. SIMULATION RESULTS

This section presents the simulation results of the proposed scheme by considering two test cases. The control system and system model are created using simulink blocks in MATLAB. With the ultimate objective to exhibit the ampleness of the proposed strategy, it is tested and differentiated from traditional methods. The lead-acid model of 48 V, 28 Ah is utilized as a battery. The switching frequency used for circuit operation is 20 kHz. The PV module is selected at a maximum peak voltage of 59 V and 960 W of power. MOSFET switches are selected to provide the bidirectional capability for the boost converter. The dc bus voltage ripple and inductor current ripple are selected as 2% and 5% respectively. The converter parameter equations are derived from [31]. The calculated simulation parameters are presented in Table I. The proposed approach simulation results for two test cases are examined below.

A. dc Bus Stabilization: Step Variation in PV Generation

The PV generation is disturbed to verify the operation HESS. Fig. 5 shows the waveform for simulation under different instances. Initially, PV supplies load demand and the additional PV power is stored in the battery. The SC current is zero at steady state operation. At t = 0.5 sec, the PV generation increases from 3.8 A to 7.6 A. SC absorbs the sudden, and the battery charges the average power from the excess power supplied by the PV. The SC absorbs the sudden excess power supplied by PV. At t = 1 sec, the PV current reduces to 5.2 A due to reduced irradiance. The additional power is used to charge the battery during the period. The load current during this period is 2 A. The time the dc bus voltage takes to settle back to the original voltage

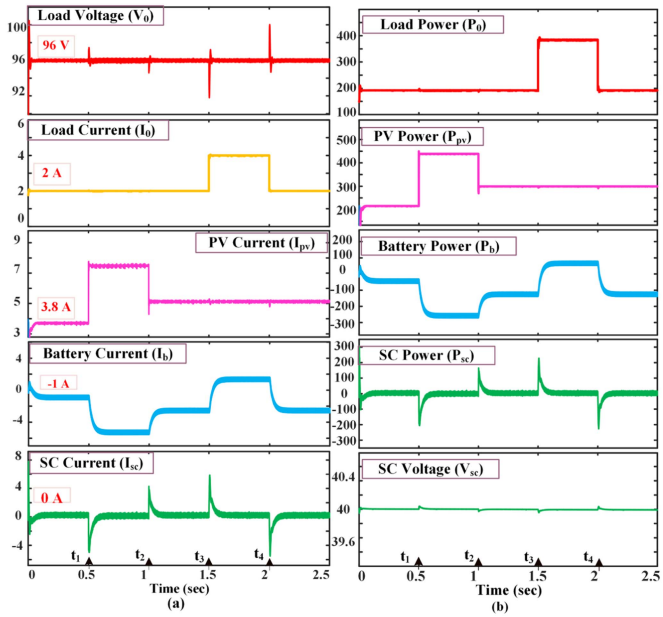

Fig. 5. Simulation Results: (a) DC bus voltage, load, PV, battery and SC currents (b) power supplied by load, PV, battery and SC, and SC voltage.

is approximately 20 msec. Also, the battery and supercapacitor currents reached the new steady-state value of 150 msec.

B. dc Bus Stabilization: Step Variation in Load Demand

The connected load across the dc bus is varied using a controlled switch. Load demand increases by 2 A in t = 1.5 sec and returns to the previous state in t = 2 sec. Since PV generation is constant, the HESS forces provide the excess load demand and battery current increases from −3 A (charging) to 2 A (discharging). The SC supplies the sudden power requirement, thereby facilitating a smooth change of battery current. The 100% change in the load current fluctuates the dc bus voltage by 4.166%. The disturbance is mitigated within 30 msec. Load power, PV power, battery power, SC power, and SC voltage are shown for different cases in Fig. 5(b). Fig. 6(a) shows an enlarged portion of load increment. The battery changes to discharging state from charging, and SC takes the transient power during the disturbance. Maximum peak ripple voltage is 4 V and the settling time is approximately 25 msec during this period.

Further, the duty variation during load disturbance is analyzed to understand the duty calculation technique. The calculated duty of battery and SC are given in Fig. 7(a) and (b). The battery shows consistent duty compared to SC. However, since SC supplies the transient and ripple power, its calculated duty has more variations during the disturbance. In summary, the dc bus oscillations due to PV variations are limited compared to load variation. Further, the battery and SC share the average and transient power during disturbances.

C. dc Bus Stabilization: SC Charging

The charging process starts once the SC operating voltage falls below 50% of the rated voltage. The controller mentioned in

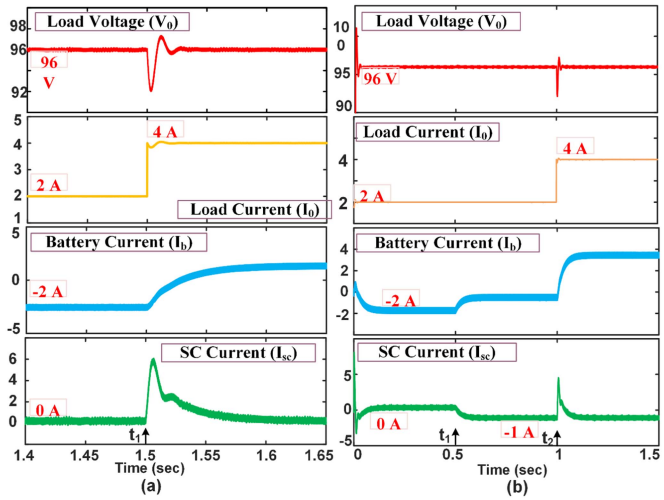

Fig. 6. Simulation Results: (a) magnified portion of load disturbance (b) Controlled charging of SC under load disturbance.

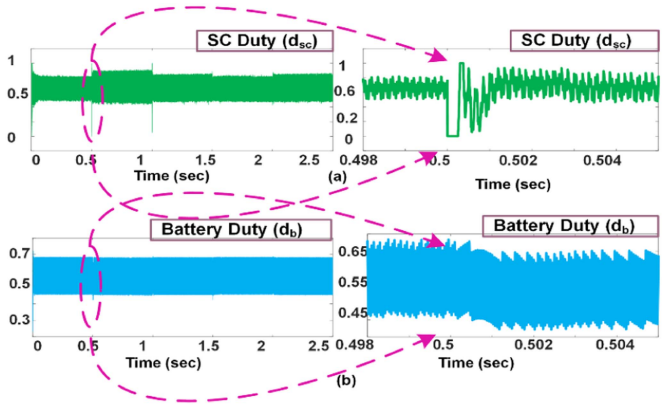

Fig. 7. Simulation results of calculated duty PV disturbance (a) SC converter duty signal (b) battery converter duty signal.

Section III-C operates when the $SC_{EN} = 1$. The charging of the SC is shown in Fig. 6(b). At t = 0.5 sec, SC_{EN} made unity and the SC starts charging. The charging does not affect the rate of change of battery current, and the fluctuation in dc bus voltage is negligible. At, $t = t_2$, 100% load change is applied. The battery provides the additional current required by the load, whereas SC provides instantaneous power without deviating from charging.

D. Comparison With Traditional Methods

The proposed hybrid control strategy is compared with traditional PI control strategies and similar topologies. A summary of the comparison is presented in Table II. The similar three-level control strategies and proposed power splitting scheme with PI controller and hybrid control strategies are compared to verify the effectiveness of the proposed method. All control strategies are simulated and compared for same power level. The traditional control strategy [16] with LPF shows high peak variation and more settling time. The second method utilizes battery current assisted power splitting strategy as shown in Fig.

TABLE II
COMPARATIVE STUDY OF HYBRID AND CONVENTIONAL CONTROL STRATEGIES

Parameters	[16]	[22]	PI+LPF [8]	Proposed
%Mp load change	6-8.5%	3.8-5%	3.8-4.6%	3.6-4.2%
%Mp PV change	2-3%	1.5-2%	1.5-1.8%	1-1.5%
Settling time (ms)	60-100	30-50	30-40	20-30
Control strategy	PI	PI	PI	Hybrid
SC voltage regulation	No	No	Yes	Yes
No. of tuning parameters	6	6	6	2

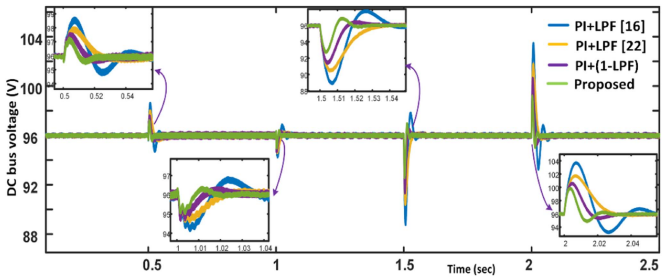

Fig. 8. Comparison waveform of load voltage with conventional methods and proposed control strategy.

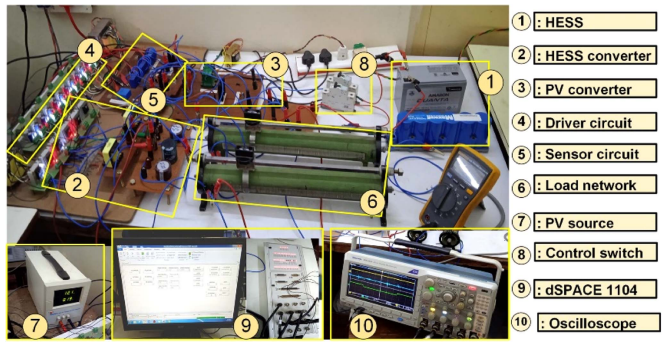

Fig. 9. Experimental setup.

2(c) [22]. This method reduces the maximum peak overshoot (Mp) below 5% and settling time (ts) below 50 msec. In all the PI control based methods, there is a trade of between Mp and ts. As a result it is difficult to attain both parameter in optimum value. The proposed power splitting strategy with PI controllers shows settling time below 40 msec and Mp below 5%. However, the above cases require three PI controllers, and their simultaneous tuning becomes complex for implementation. The use of prediction and PI together reduces the lag effect on the control system and improves the dc bus voltage control dynamics. As a result, the proposed method shows a 43% reduction in peak overshoot and a 62% reduction in maximum settling time compared to the traditional approach [16]. Peak overshoot of 4.2% and settling time of 30 ms are exhibited by the proposed hybrid controller-operated dc microgrid. Fig. 8 shows the comparison of different control strategies.

V. HARDWARE IMPLEMENTATION AND DISCUSSION

A hardware prototype has been developed to test the proposed hybrid controller for the PV dc microgrid depicted in Fig. 9.

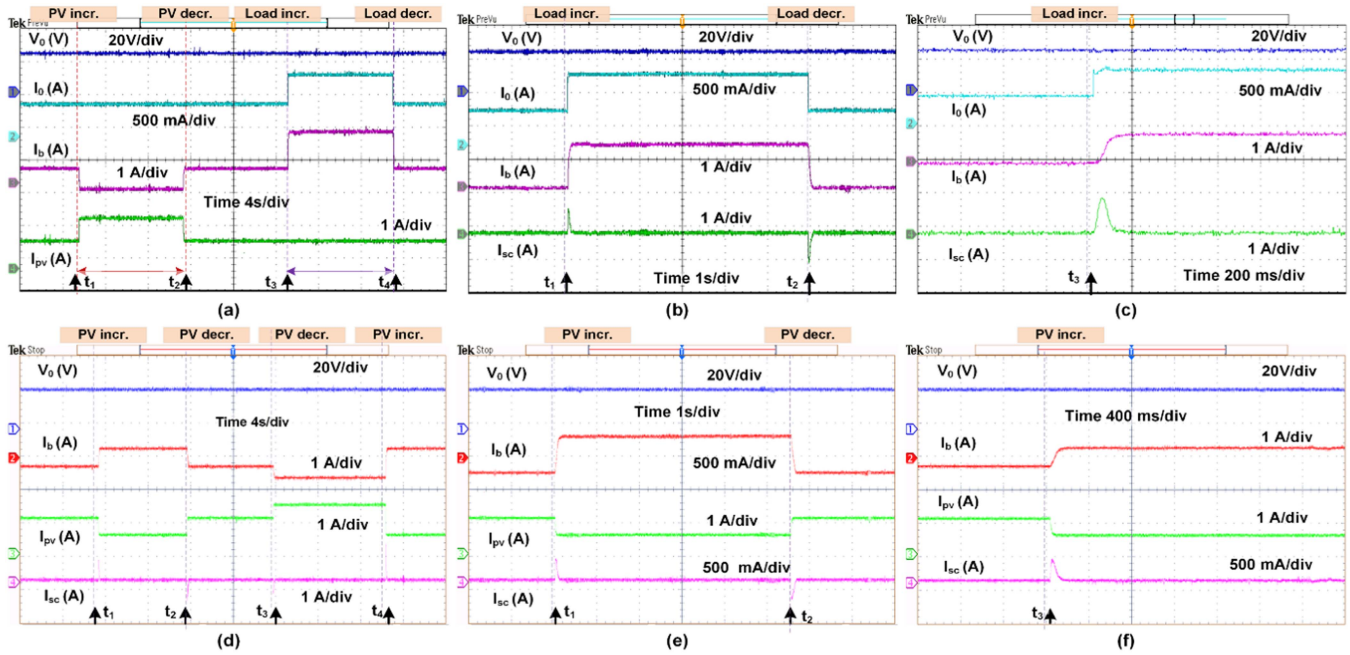

Fig. 10. Experimental results: system performance with (a) PV irradiance and load change (b) SC and battery current sharing during load change (c) enlarged view of load increment (d) operation under PV irradiance variation (e) load voltage during irradiance variation (f) enlarged view of PV disturbance.

TABLE III
DETAILS OF EXPERIMENTAL STUDY

S.No	Parameter	Value
1	DC bus voltage	24 V
2	Battery storage	12 V, 7 Ah
3	Emulated PV source	12V, 5A
4	SC unit	16 V, 58 F, 20 A
5	Filter inductances (L_{PV}, L_b, L_{sc})	4.1 mH, 2 mH, 2 mH
6	Load capacitance	220 μF
7	Switching frequency, (f_{sw})	20 kHz

The dSPACE DS1104 real-time platform is used to develop the controller for this experiment. A regulated power supply is manipulated as a PV source in this experiment [22]. A boost converter is employed to control the PV currents. The battery and SC rating is 12 V, 7Ah lead-acid type, and Maxwell BMOD0058 16 V, 58F. The function of the HESS microgrid is tested in several modes of operation. The nominal dc bus voltage is selected as 24 V. The converter parameters for dc microgrid system is designed for 150 W. The parameter details of experimental setup is summarized in Table III.

A. Change in Connected Load

Here, the load variations are created by connecting two rheostats in parallel through a mechanical switch. The overall system performance was tested with load and source disturbances as demonstrated in Fig. 10(a). At t_3 and t_4, load disturbances are applied. Primarily, the PV supplies the load demand, and the battery current is 0.4 A. At t_3, the load current increases from 0.5 A to 1.1 A. The battery current changes from 0.4 A to 1.2 A to meet the load demand as power supplied by PV is constant. At t_4, the load demand is reduced to 0.5 A. The SC current is zero during the steady-state period, and supplies/absorbs transient current at the time of disturbances, as depicted in Fig. 10(b). Fig. 10(c) shows the enlarged load increment and decrement section. It is evident from the results that the dc bus voltage has fewer oscillations during load disturbance. The battery voltage during different load disturbances shows no variation due to disturbances, as shown in Fig. 11(b). Battery compensates only the average power demand, and the SC balances for transient power.

B. Change in PV Generation

When the PV generation changes, the HESS charge or discharge load depends on the demand. Fig. 10(a) summarises the change in PV generation. Initially, PV generation is more, and the battery current shows a negative current due to charging. At t_1, the PV current reduces from 1.1 A to 0.6 A and the battery changes from charging to discharging. At t_2, PV current increases to 1.1 A and again increases to 1.5 at t_3. The battery starts to charge as the PV generation exceeds load demand during this period. At t_3, the battery is charged with a current of 0.6 A. The SC supplies/absorb the transient current in all PV changes, and the battery balances the average current. At t_4, The PV current changes from 1.5 A to 0.6 A, forcing the battery to discharge more power. As a result, SC supplies transient current with a peak of 1 A, and the battery starts discharging with 0.3 A. A further magnified portion of PV disturbance is shown in Fig. 10(b) and (c). The waveforms show that the dc bus voltage is stabilized under various disturbances, and SC absorbs the transient power according to the control strategy.

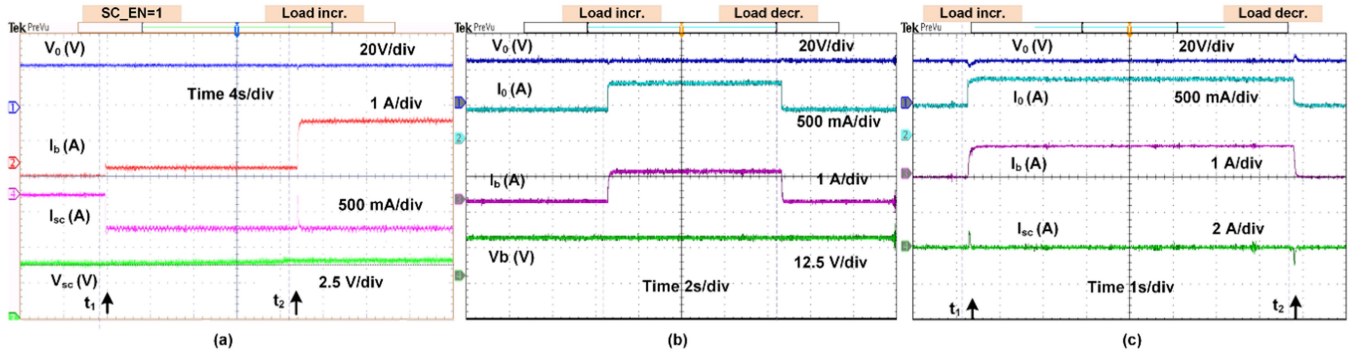

Fig. 11. Experimental results: (a) charging of SC under load disturbance (b) battery voltage during disturbance (c) operation of DC microgrid with PI-LPF control strategy.

C. Charging of SC

To verify the SC charging scheme, SC_{EN} is made unity at t_1. Initially, the battery charges from the dc bus with -0.4 A, SC current is 0 A, SC voltage is 8 V, and load voltage is 24 V. Then, the charging of SC is started at t_1 with 0.5 A charging current as shown in Fig. 11(a). Finally, at t_2, load disturbance is applied with an increment of 0.5 A in load current. Consequently, the battery current rises to 1 A to meet the steady state power demand, and the SC supplies the transient power. As a result, the impact of load disturbance during SC charging on dc bus voltage is minimized. In summary, the SC can support the battery during charging and supply the transient power without affecting the dc microgrid operation.

D. Comparison With Conventional PI Method

The conventional PI-LPF based control of HESS has a simple structure compared to the proposed hybrid controller. The proposed method requires a minimum of five sensors to implement the hardware, whereas the conventional requires four sensors to implement it with SC charging scheme. Fig. 11(c) shows the experimental waveforms for conventional PI-based dc microgrid. Initially, the battery is charging from the dc bus, and the load demand is 0.4 A. At t_1, the load demand is increased by 100%. The load voltage varies is 1.8 V to 2 V, whereas the proposed strategy shows voltage variation of less than 0.5 V. The waveforms demonstrate that the conventional method has higher dc bus voltage peaks than the proposed hybrid control strategy.

VI. Conclusion

In this article, a hybrid controller for HESS with a new power splitting scheme is proposed for an isolated dc microgrid. The dc bus voltage is regulated using the PI controller, and the power splitting scheme can generate battery reference current without the direct aid of LPF. The combination of hybrid control and power splitting scheme improves the dynamic power-sharing and dc bus voltage regulation of the dc microgrid. The parameter dependence of duty calculation is minimal for the battery, and the predicted duty tends to reach upper saturation for SC at less than 50% SC voltage. Hence, an SC charging controller is incorporated to charge the SC while operating below 50% SC-rated voltage. The steady-state and dynamic performance of the autonomous microgrid is accessed by offline simulation and verified experimentally using a laboratory prototype. Compared to the conventional HESS control strategy, the proposed system shows a 43% reduction in peak overshoot and a 62% reduction in maximum settling time. The experimental study is conducted for different power levels, and the results reflect the simulation study. In summary, the suggested hybrid controller integrated autonomous dc microgrid is capable of 1) quick dynamic voltage regulation, 2) proper power sharing between the battery and SC with minimized delay, 3) reduces the complexity in modelling and parameter tuning for implementation and 4) simultaneous operation of SC charging and dc bus voltage regulation. Therefore, combining PI with predictive control enhances dynamics and guarantees proper power sharing of HESS in an isolated dc microgrid.

References

[1] S. Vazquez, S. M. Lukic, E. Galvan, L. G. Franquelo, and J. M. Carrasco, "Energy storage systems for transport and grid applications," *IEEE Trans. Ind. Electron.*, vol. 57, no. 12, pp. 3881–3895, Dec. 2010.

[2] T. Dragičević, J. M. Guerrero, J. C. Vasquez, and D. Škrlec, "Supervisory control of an adaptive-droop regulated DC microgrid with battery management capability," *IEEE Trans. Power Electron.*, vol. 29, no. 2, pp. 695–706, Feb. 2014.

[3] H.-S. Lee and J.-J. Yun, "High-efficiency bidirectional buck–boost converter for photovoltaic and energy storage systems in a smart grid," *IEEE Trans. Power Electron.*, vol. 34, no. 5, pp. 4316–4328, May 2019, doi: 10.1109/TPEL.2018.2860059.

[4] J. Tobajas, F. Garcia-Torres, P. Roncero-Sánchez, J. Vázquez, L. Bellatreche, and E. Nieto, "Resilience-oriented schedule of microgrids with hybrid energy storage system using model predictive control," *Appl. Energy*, vol. 306, Jan. 2022, Art. no. 118092.

[5] D. Vijay M, B. Singh, and G. Bhuvaneswari, "Grid-tied battery integrated wind energy generation system with an ability to operate under adverse grid conditions," *IEEE Trans. Ind. Appl.*, vol. 56, no. 6, pp. 6882–6891, Nov./Dec. 2020, doi: 10.1109/TIA.2020.3024156.

[6] C. Cheng, A. Blakers, M. Stocks, and B. Lu, "Pumped hydro energy storage and 100% renewable electricity for East Asia," *Glob. Energy Interconnection*, vol. 2, no. 5, pp. 386–392, Oct. 2019.

[7] H. F. Gharibeh, A. S. Yazdankhah, M. R. Azizian, and M. Farrokhifar, "Online energy management strategy for fuel cell hybrid electric vehicles with installed PV on roof," *IEEE Trans. Ind. Appl.*, vol. 57, no. 3, pp. 2859–2869, May/Jun. 2021, doi: 10.1109/TIA.2021.3061323.

[8] C. R. Arunkumar, U. B. Manthati, and S. Punna, "Supercapacitor voltage based power sharing and energy management strategy for hybrid energy storage system," *J. Energy Storage*, vol. 50, 2022, Art. no. 104232.

[9] Q. Xu, J. Xiao, X. Hu, P. Wang, and M. Y. Lee, "A decentralized power management strategy for hybrid energy storage system with autonomous bus voltage restoration and state-of-charge recovery," *IEEE Trans. Ind. Electron.*, vol. 64, no. 9, pp. 7098–7108, Sep. 2017.
[10] L. Zhang, X. Hu, Z. Wang, F. Sun, and D. G. Dorrell, "A review of supercapacitor modeling, estimation, and applications: A control/management perspective," *Renewable Sustain. Energy Rev.*, vol. 81, pp. 1868–78, Jan. 2018.
[11] M. C. Joshi and S. Samanta, "Improved energy management algorithm with time-share-based ultracapacitor charging/discharging for hybrid energy storage system," *IEEE Trans. Ind. Electron.*, vol. 66, no. 8, 6032–6043, Aug. 2019.
[12] C. R. Arunkumar, U. B. Manthati, and S. Punna, "Supercapacitor-based transient power supply for DC microgrid applications," *Elect. Eng.*, vol. 104, no. 2, pp. 463–472, 2022.
[13] S. Barcellona, L. Piegari, and A. Villa, "Passive hybrid energy storage system for electric vehicles at very low temperatures," *J. Energy Storage*, vol. 25, Oct. 2019, Art. no. 100833.
[14] Q. Zhang and G. Li, "Experimental study on a semi-active battery-supercapacitor hybrid energy storage system for electric vehicle application," *IEEE Trans. Power Electron.*, vol. 35, no. 1, pp. 1014–1021, Jan. 2020.
[15] Z. Song et al., "Multi-objective optimization of a semi-active battery/supercapacitor energy storage system for electric vehicles," *Appl. Energy*, vol. 135, pp. 212–224, Dec. 2014.
[16] W. Jing et al., "A comprehensive study of battery-supercapacitor hybrid energy storage system for standalone PV power system in rural electrification," *Appl. Energy*, vol. 224, pp. 340–356, 2018.
[17] C. R. Arunkumar and U. B. Manthati, "Design and small signal modelling of battery-supercapacitor HESS for DC microgrid," in *Proc. IEEE TENCON Region 10 Conf.*, 2019, pp. 2216–2221.
[18] D. B. W. Abeywardana, B. Hredzak, V. G. Agelidis, and G. D. Demetriades, "Supercapacitor sizing method for energy-controlled filter-based hybrid energy storage systems," *IEEE Trans. Power Electron.*, vol. 32, no. 2, pp. 1626–1637, Feb. 2017, doi: 10.1109/TPEL.2016.2552198.
[19] S. Punna, U. B. Manthati, and A. Chirayarukil Raveendran, "Modeling, analysis, and design of novel control scheme for two-input bidirectional DC-DC converter for HESS in DC microgrid applications," *Int. Trans. Elect. Energy Syst.*, vol. 4, 2021, Art. no. e12774.
[20] N. R. Tummuru, M. K. Mishra, and S. Srinivas, "Dynamic energy management of renewable grid integrated hybrid energy storage system," *IEEE Trans. Ind. Electron.*, vol. 62, no. 12, pp. 7728–7737, Dec. 2015.
[21] U. Manandhar et al., "Energy management and control for grid connected hybrid energy storage system under different operating modes," *IEEE Trans. Smart Grid.*, vol. 10, no. 2, 1626–1636, Mar. 2019.
[22] S. K. Kollimalla, M. K. Mishra, A. Ukil, and H. B. Gooi, "DC grid voltage regulation using new HESS control strategy," *IEEE Trans. Sustain. Energy*, vol. 8, no. 2, pp. 772–781, Apr. 2017, doi: 10.1109/TSTE.2016.2619759.
[23] Y. Zhou et al., "A predictive set-point modulation energy management strategy for hybrid energy storage systems," *IEEE Trans. Ind. Appl.*, vol. 55, no. 6, 6266–6277, Nov./Dec. 2019.
[24] B. R. Ravada and N. R. Tummuru, "Control of a supercapacitor-battery-PV based stand-alone DC-microgrid," *IEEE Trans. Energy Convers.*, vol. 35, no. 3, 1268–1277, Sep. 2020.
[25] E. M. Asensio, G. A. Magallán, C. H. De Angelo, and F. M. Serra, "Energy management on battery/ultracapacitor hybrid energy storage system based on adjustable bandwidth filter and sliding-mode control," *J. Energy Storage*, vol. 30, Aug. 2020, Art. no. 101569.
[26] P. Singh and J. S. Lather, "Dynamic current sharing, voltage and SOC regulation for HESS based DC microgrid using CPISMC technique," *J. Energy Storage*, vol. 30, Aug. 2020, Art. no. 101509.
[27] " Z. Cheng et al., "A novel cascaded control to improve stability and inertia of parallel buck-boost converters in DC microgrid," *Int. J. Elect. Power Energy Syst.*, vol. 119, 2020, Art. no. 105950, doi: 10.1016/j.ijepes.2020.105950.
[28] R. Bhosale and V. Agarwal, "Fuzzy logic control of the ultracapacitor interface for enhanced transient response and voltage stability of a DC microgrid," *IEEE Trans. Ind. Appl.*, vol. 55, no. 1, pp. 712–720, Jan./Feb. 2020.
[29] A. Katnapally, U. B. Manthati, A. Chirayarukil Raveendran, and S. Punna, "A predictive power management scheme for hybrid energy storage system in electric vehicle," *Int. J. Circuit Theory Appl.*, vol. 49, no. 11, pp. 3864–3878, 2021.
[30] S. Chen, Q. Yang, J. Zhou, and X. Chen, "A model predictive control method for hybrid energy storage systems," *CSEE J. Power Energy Syst.*, vol. 7, no. 2, pp. 329–338, Mar. 2021, doi: 10.17775/CSEE-JPES.2019.01960.
[31] R. W. Erickson and D. Maksimovic, *Fundamentals of Power Electronics*. Berlin, Germany: Springer, 2007.

Arunkumar C R (Graduate Student Member, IEEE) received the B.Tech. degree in electrical and electronics engineering and the M.Tech. degree in power electronics and control from Mahatma Gandhi University, Kottayam, India, in 2013 and 2016, respectively, and the Ph.D. degree in electrical engineering from the National Institute of Technology-Warangal, Telangana, India, in 2022. He is currently with Tata Elxsi as a Senior Engineer.

Udaya Bhasker Manthati (Member, IEEE) born in the year 1980. He received the B.Tech. degree in electrical & electronics engineering and the M.E. degree in power electronics & drives in 2003 and 2006, respectively, and the Ph.D. degree in electrical engineering from the Technical University of Catalonia, Barcelona, Spain, in 2011. Since 2022, he has been an Associate Professor with the Department of Electrical Engineering, National Institute of Technology-Warangal (NIT-W), Warangal, India. During 2011–2022, he was an Assistant Professor with Manipal University Jaipur, Jaipur, India, and NIT-W. During 2007–2011, he was a Research Assistant with CITCEA-UPC, Spain. He has author and co-author for various national and international repute journals and conferences. His research interests include DC-DC converters, power electronics applications to micro grid and smart grid technologies, energy storage systems, digital control, and synchrotron power supplies. He was the recipient of the Synchrotron Light Laboratory-UPC Fellowship during 2007–2010 and Deutschen Akademischen Austauschdienstes (DAAD) stipend from FH-Deggendorf, Germany in the year 2007. He was also the recipient of Two Ph.D.'s under his supervision and three Ph.D.'s are pursuing. So far ten FDP's are organized in electrical engineering applications. He has written two book chapters of international repute. He is currently supervising M.Tech. and Ph.D. thesis in the domain of hybrid energy storage systems and digital control.